Amorphous Zr-Based Foams with Aligned, Elongated Pores

MARIE E. COX, SUVEEN N. MATHAUDHU, K. TED HARTWIG, and DAVID C. DUNAND

Interpenetrating phase composites are created by warm equal channel angular extrusion (ECAE) of blended powders of amorphous $Zr_{58.5}Nb_{2.8}Cu_{15.6}Ni_{12.8}Al_{10.3}$ (Vit106a) and a crystalline ductile metal (Cu, Ni, or W). Subsequent dissolution of the continuous metallic phase results in amorphous Vit106a foams with ~40 pct aligned, elongated pores. The extent of Vit106a powder densification in the composites improves with the strength of the crystalline metallic powder, from low for Cu to high for W, with a concomitant improvement in foam compressive strength, ductility, and energy absorption.

DOI: 10.1007/s11661-009-0039-3

I. INTRODUCTION

BULK metallic glasses (BMGs) have very high specific strength but lack room-temperature plasticity and fail catastrophically from highly localized shear bands.[1,2] Improvements in fracture stress and ductility can be achieved by arresting shear bands through addition of a ductile metallic second phase.[3,4] Shear band arrest can also be achieved by pores, leading to improved compressive ductility in porous BMGs.[5] At high porosity, BMG foams exhibit an interconnected network of thin amorphous metal struts deforming in bending where shear-band stabilization becomes active: as strut diameter decreases, shear bands become shallower, thus relaxing a smaller volume and enabling higher band density while creating smaller shear offsets, which reduce the probability of crack nucleation. This results in very high compressive ductility[6] with non-catastrophic damage accumulation.[7] As reviewed recently,[8,9] BMG foams have been created by the liquid route for alloys based on Pd,[10,11] Zr,[6,12,13] Fe,[14] Ti,[15] La,[16] and Mg.[17] The high contamination tendency and limited casting diameters of BMG alloys are major limitations when using liquid state processing to create BMG foams.

These issues have been addressed by various authors by using amorphous metallic powders to create porous metallic glasses. Partial sintering of amorphous powders by spark plasma sintering resulted in amorphous Zr-based foams with 14 to 33 pct porosity.[18] Consolidation by warm extrusion or hot pressing of amorphous powders blended with space-holder particles, which are subsequently removed, has been used to create amorphous Ni-based foams with porosity $p = 40$ pct using brass as a space holder,[19] Zr-based foams with $p = 70$ pct using salt as a space holder,[20] and Cu-based nanoporous foams with $p = 25$ pct using crystalline Cu.[21] Consolidation by hot isostatic pressing of amorphous powders and a blowing agent (magnesium carbonate) followed by expansion of the consolidated precursor has produced amorphous Pd-based foams with porosities up to $p = 86$ pct.[22] Of these investigations, only two reported mechanical properties for the foams. First, the Ni-based, extruded foam ($p = 40$ pct)[19] exhibited a compressive stress strain curve (with the loading direction parallel to the extrusion direction) with a fracture strength of 356 MPa and a plastic strain of ~3.2 pct (at which point testing was interrupted due to a load drop of 30 pct); scanning electron microscopy (SEM) imaging of the deformed foam showed shear bands within the parallel struts and fracture of bundles of individual struts. The authors attributed the low plasticity to the sharp notches created by the elongated pores.[19] Second, the Pd-based foam[22] with $p = 4$, 40, and 86 pct showed yield strengths of 650, 225, and 25 MPa, respectively, and plastic deformation of ~0, >20, and 80 pct, respectively.

Equal channel angular extrusion (ECAE) has two main advantages over other powder extrusion methods: (1) there is a small change in the billet cross section allowing multiple extrusions to be performed and (2) the punch pressure is lower than standard extrusion techniques for the same amount of imparted strain.[23] Equal channel angular extrusion has been used previously to densify BMG powders with and without a second phase,[24–28] but to our knowledge, these second phases have not been removed to create a foam. Here, we use ECAE to consolidate a mixture of Zr-based bulk metallic glass and crystalline metallic powders into a composite, from which the metallic phase is dissolved to

MARIE E. COX, Graduate Student, and DAVID C. DUNAND, Professor, are with the Department of Materials Science and Engineering, Northwestern University, Evanston, IL, 60208. Contact e-mail: dunand@northwestern.edu SUVEEN N. MATHAUDHU, Researcher, is with the United States Army Research Laboratory, Weapons and Materials Research Directorate, Aberdeen Proving Ground, MD 21005. K. TED HARTWIG, Professor, is with the Department of Mechanical Engineering, Texas A&M University, College Station, TX 77843.

This article is based on a presentation given in the symposium "Bulk Metallic Glasses VI," which occurred during the TMS Annual Meeting, February 15–19, 2009, in San Francisco, CA, under the auspices of TMS, the TMS Structural Materials Division, TMS/ASM: Mechanical Behavior of Materials Committee.

Published online: 24 November 2009

create porosity. We report on the structure and mechanical properties of these foams, which show aligned, elongated pores, as a result of the ECAE densification process.

II. EXPERIMENTAL PROCEDURES

Using processing parameters developed by Mathaudhu *et al.*,[25] Vit106a ($Zr_{58.5}Nb_{2.8}Cu_{15.6}Ni_{12.8}Al_{10.3}$) powders (38 to 105 μm, fabricated at the Materials Processing Center of Ames Laboratory by high pressure gas atomization) were mixed with 60 vol pct tungsten, nickel, or copper powders (45 to 106 μm). The powder blends were poured in $19 \times 19 \times 90$ mm^3 Ni cans, which were vacuum sealed by electron-beam welding. The cans were then pushed at a rate of 0.5 mm/s through a 90 deg ECAE die whose walls were heated to 420 °C (within Vit106a's supercooled liquid region, $T_g = 401$ °C, $T_x = 499$ °C) with no counterpressure.[29] Each can was instrumented with two thermocouples along the billet centerline (Figure 1), which, together with the tooling thermocouple, were used to monitor continuously the can temperature during extrusion. After a single pass, consolidated composites were electrodischarge machined from the center of the extruded billet and polished into $2 \times 2 \times 4$ mm^3 compression samples, with their long dimension in the direction of extrusion.

Removal of the Cu and Ni phases in the composites (referred to as Vit/Cu, Vit/Ni) was achieved by exposure to an acid solution (35 vol pct concentrated HNO_3 in water) for 40 and 60 minutes, respectively. Removal of the W phase from the Vit/W composites required 20 to 32 hours in an electrochemical cell with a solution of 1.5 M KOH and a voltage of 5 V. In the following, Vit106a foams resulting from the dissolution of Cu, Ni, and W are referred to as VitCu, VitNi, and VitW foams, respectively. After dissolution, foams were coated with a thin layer of vacuum grease and their porosity was determined by the Archimedes method, where the sample mass is measured in air and in water.

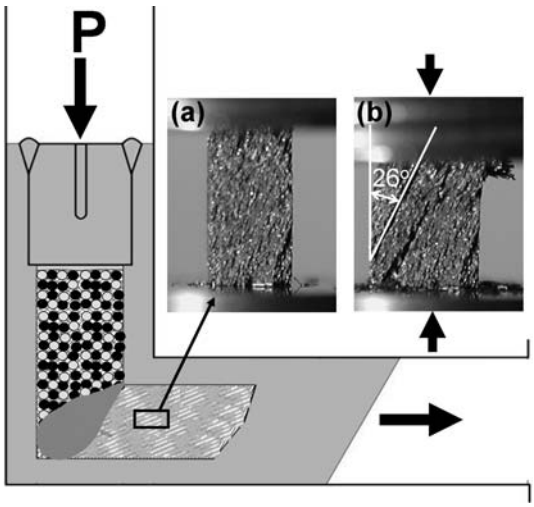

Fig. 1—Schematic of powder billet during ECAE processing and the resulting VitNi foam (*a*) before loading and (*b*) after 24 pct compressive strain, showing cracks forming at 22 to 28 deg to the axis of loading.

To determine the compressive properties of the Vit106a foams, two specimens of each foam type were uniaxially compressed in the direction of extrusion under displacement control at a nominal strain rate of 5×10^{-4} s^{-1}. Load train compliance corrections were made using data collected on an Al calibration standard before and after each test, and the data are presented as engineering stress and strain. After compression testing, a portion of the fractured samples were crushed and subjected to X-ray diffraction using Cu K_α radiation.

III. RESULTS

A. *Microstructure*

An optical micrograph of a transverse cross section of the Vit/Cu composite (Figure 2(a)) shows good densification of the Cu and Vit106a powders. The Vit106a phase retained the original rounded shape of the powders, while the Cu phase densified and flowed to become the "matrix" of the composite. A micrograph for the Vit/Ni composite (Figure 2(b)) shows the same good densification but deformation of both Vit106a and Ni phases. A micrograph for the Vit/W composite (Figure 2(c)) shows that the Vit106a has flowed extensively, forming the "matrix" of the composite, while the W phase is also highly elongated along an angle of ~26 deg with respect to the extrusion direction.

The X-ray diffraction patterns for the VitCu and VitNi foams (Figure 3) showed no measurable crystalline phases, confirming that no significant devitrification occurred during the powder consolidation step and that all Cu and Ni were removed during the dissolution step. By contrast, the VitW foams show a very slight peak at $2\theta = 40.3$ deg, which corresponds to the (110) reflection for W. These trace amounts of W in the foam, possibly in the form of rare isolated W powders not removed during the dissolution process, are not sufficient to affect the measured porosity.

The SEM micrographs of the fracture surfaces of the VitCu foam ($p = 57$ and 64 pct) show that individual Vit106a powders, while bonded to each other, remain distinguishable (Figure 4(a)); they are only slightly elongated in the shear direction, forming a 22 to 28 deg angle, as measured from optical micrographs, with the extrusion direction. The SEM images of the VitNi foams ($p = 57$ and 59 pct) show more extensive deformation and bonding of the Vit106a powders, which are still partially recognizable and form a network of cell walls (Figure 4(b)) aligned in the shear direction. Individual powders are visible in polished cross sections of the VitNi foams (Figures 5(a) and (b)). By contrast, Figure 4(c) shows the fracture surface of the VitW foam ($p = 59.5$ and 63 pct), which is characterized by cell walls with no clearly recognizable powders. Elongated pores in cross sections of the VitW foam (Figures 5(c) and (d)) have 25- to 150-μm width and 80- to 350-μm lengths.

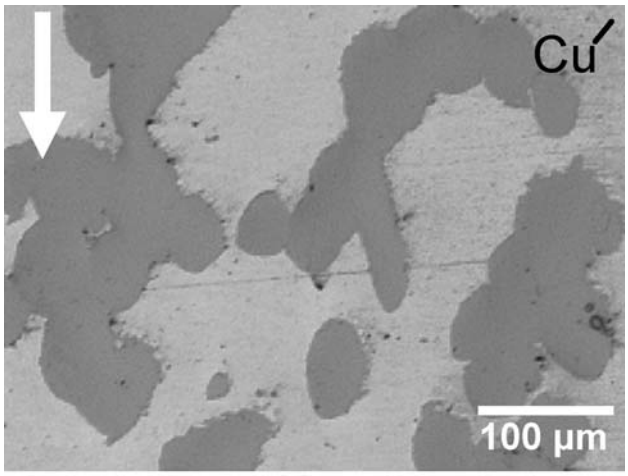

(a)

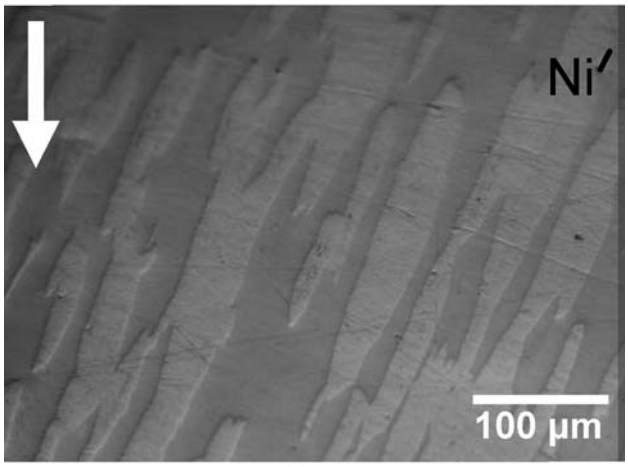

(b)

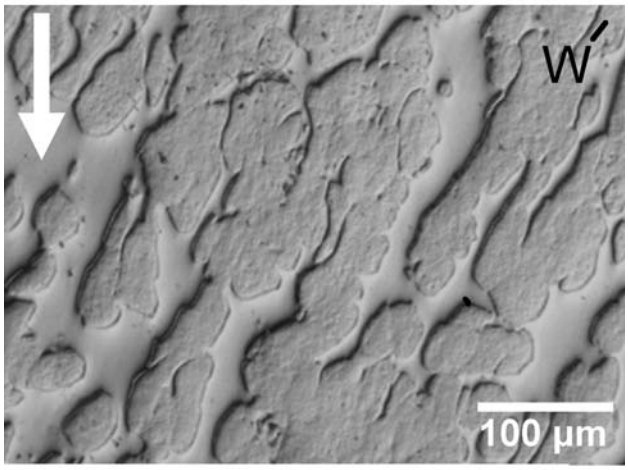

(c)

Fig. 2—Optical micrographs of cross sections of composites (*a*) Vit/Cu with Cu as the lighter phase, (*b*) Vit/Ni with Ni as the lighter phase, and (*c*) Vit/W with W as the darker phase. Arrows indicate direction of extrusion.

B. *Mechanical Properties*

Figure 6(a) shows the engineering compressive stress-strain curves for the two VitCu foams (labeled 1 and 2) with porosity $p = 57$ and 64 pct, respectively. The curves are characterized by a short elastic range, a long plateau at 0.3 to 1 MPa, and a final densification branch. Spalling from the top of the samples began between 3 and 5 pct strain and continued throughout the compression test, explaining the numerous stress drops visible in the curves. The large stress drop visible at a strain of 40 pct for foam VitCu-2 with $p = 64$ pct corresponded to a large piece of the sample breaking off the top of the test specimen. The maximum stresses were 0.5 and 1.8 MPa for the VitCu-1 and -2 foams, respectively.

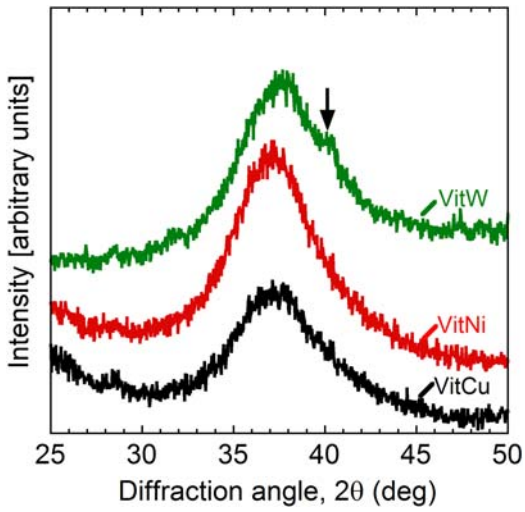

Fig. 3—XRD patterns of the three foams showing a broad amorphous hump. The arrow highlights a small rise in the amorphous hump corresponding to a tungsten peak.

As shown in Figure 6(b), the stress-strain curves of the VitNi-1 and -2 foams ($p = 57$ and 59 pct, respectively) showed a large drop in stress after yielding (peak stresses of 13.5 and 6 MPa) followed by a plateau stress at 1 to 2 MPa until the sample fractured or densified. Between 4 and 7 pct strain, both samples developed visible cracks at 22 to 28 deg angles with respect to the loading axis. At higher strains, additional cracks formed that propagated through the entire sample on parallel planes that were also at ~26 deg to the loading direction. Figure 1(b) shows these large cracks in the VitNi-2 foam at 24 pct strain. Between 40 and 50 pct strain, the cracks had visibly propagated through the sample and sections of foam became detached from the load-bearing portion of the sample. Throughout testing, minor spalling occurred from the top of the sample.

Figure 6(c) show the stress strain curves of the VitW-1 and -2 foams ($p = 59.5$ and 63 pct, respectively), which exhibit a loading stiffness of 4.1 and 3.4 GPa, respectively; stiffness could not be determined reliably for the other foams, due to the shortness of their elastic range. Yield strengths of the VitW-1 and -2 foams are 61 and 62 MPa, respectively, and are followed by a drop in stress of ~25 MPa, leading to a plateau region followed by densification where the stress increases rapidly. During the tests, the samples showed signs of macroscopic shear and cracking along the planes at 22 to

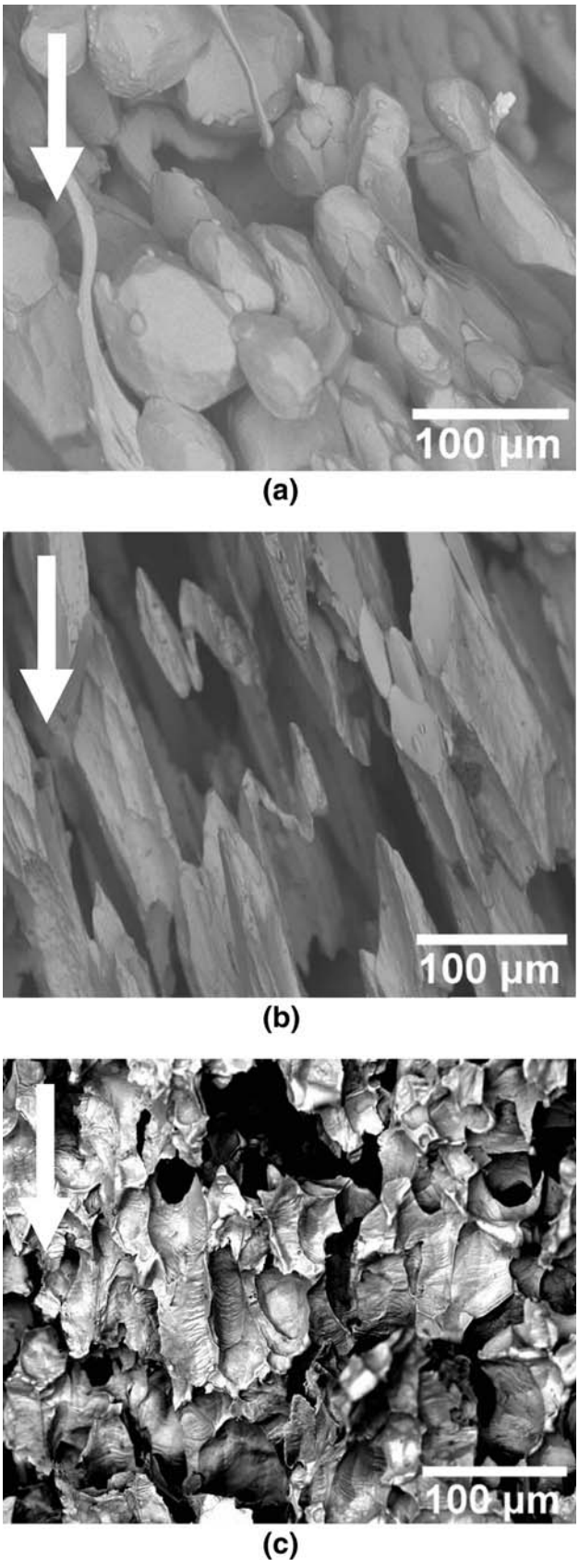

Fig. 4—SEM images of fracture surfaces of (*a*) VitCu, (*b*) VitNi, and (*c*) VitW foams. The white arrows indicate the direction of extrusion.

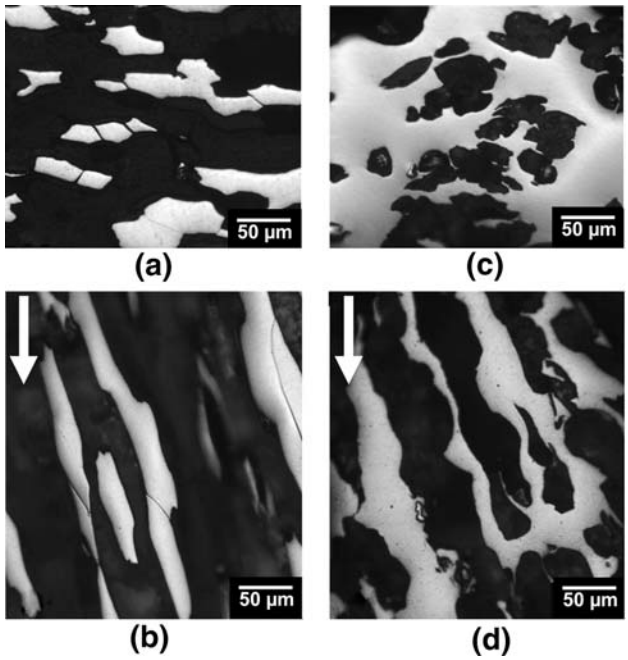

Fig. 5—Optical micrographs of cross sections for the VitNi foam with plane of polish (*a*) perpendicular and (*b*) parallel to the extrusion direction and for the VitW foam with plane of polish (*c*) perpendicular and (*d*) parallel to the extrusion direction. The white arrows indicate the direction of extrusion.

29 deg to the loading direction, but no large pieces were expelled as in the other foams. Minimal spalling occurred at the bottom of the sample at high strains. The crushing energies (determined by measuring the area under the stress-strain curve up to 65 pct strain) are 32 and 38 MJ/m^3 for the VitW-1 and -2 foams, respectively.

IV. DISCUSSION

A. *Processing and Microstructure*

Powder densification during ECAE occurs through shear stresses developed while the can is pushed through the die: for a 90 deg die angle, the shear plane is expected to form a 22 deg angle with respect to the direction of extrusion,[30] although angle variations are expected because of wall friction and variation in tooling geometries.[31] Once the crystalline phase was removed, the SEM and optical images of the foams show that the powders deformed along shear planes that form 22 to 28 deg angle with respect to the direction of extrusion (which is also the uniaxial compression axis during the subsequent compressive testing of samples). Thus, the foams with aligned, elongated pores are tested in a direction forming a 22 to 28 deg angle with the main orientation of the pores. Further extrusions, if they can occur without crystallizing the composites, can lead to a variety of pore geometries, *e.g.*, elongation along planes forming angles of 13 and 7 deg with respect to the extrusion direction, for the 2A and 4A routes, respectively.[30]

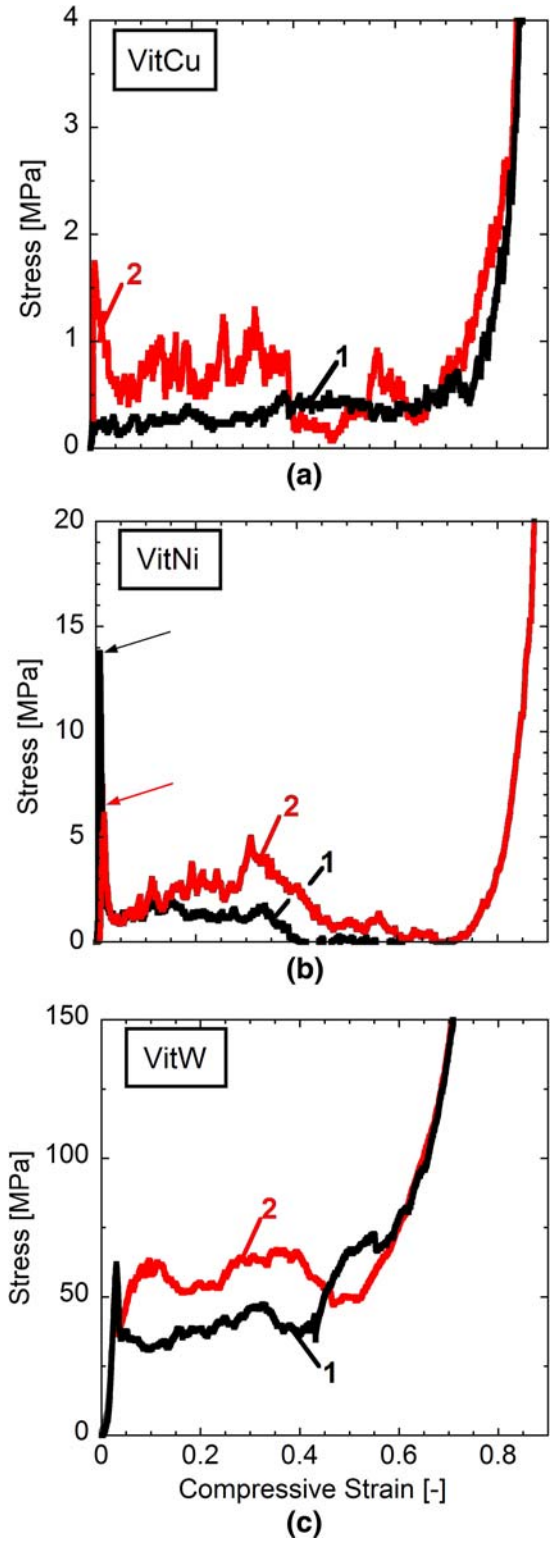

Fig. 6—Uniaxial compressive stress-strain curves for (*a*) VitCu, (*b*) VitNi, and (*c*) VitW foams.

The strength of the crystalline powders has a strong effect on the structure of the composites and the resulting foams. The VitCu foams are characterized by a network of weakly bonded Vit106a powders (Figure 4(a)), leading to a low plateau strength (Figure 6(a)). This lack of Vit106a powder bonding during ECAE is attributed to the low flow strength of Cu (~70 MPa at the ECAE temperature of 420 °C[32]) as compared to that of Vit106a, estimated as 125 to 320 MPa[33] for a similar amorphous alloy ($Zr_{65}Al_{10}Ni_{10}Cu_{15}$) at 420 °C for strain rates of 0.03 to 0.3 s^{-1}. The strain rate sensitivity of $Zr_{65}Al_{10}Ni_{10}Cu_{15}$ at the processing temperature is very high ($m = 0.4$ to 0.85) as compared to that of crystalline metals $m \sim 0.1$.[33,34] It is apparent from Figure 2(a) that, during extrusion, the weak Cu powders densified and flowed much more readily than the harder Vit106a powders, which were thus engulfed within a Cu matrix. Thus, after Cu removal, only limited deformation of the Vit106a powder along the shear plane at a 22 to 26 deg angle to the horizontal extrusion plane and weak powder connectivity are seen in the Vit106a foams.

As shown in Figures 4(b) and 5(a) and (b), the VitNi foams consist of powder particles that are more elongated and better connected with each other than the VitCu foams, thus forming true cell walls. At the 420 °C extrusion temperature, Ni has a flow strength of ~100 MPa for strain rates of 0.03 to 0.3 s^{-1}.[32] The higher flow strength of Ni, as compared to Cu, results in increased deformation of the Vit106a powders during extrusion, as visible in Figure 2(b). However, individual Vit106a powders, despite being strongly elongated by the ECAE process, are still clearly visible in Figure 5(a) and (b).

Finally, in the Vit/W composite (Figure 2(c)) and the resulting VitW foams (Figures 4(c) and 5(c) and (d)), the Vit106a powders have completely densified and are not individually recognizable. The higher flow strength of tungsten, ~350 MPa,[32] resulted in the weaker Vit106a (125 to 320 MPa[33]) densifying and flowing around the harder W particles, which also elongated, as can be deduced from the elongated shape of the pores in the VitW foam (Figure 5(d)) and the original composite micrographs (Figure 2(c)). The Vit106a powders densified to become a continuous phase with no distinguishable powder boundaries (Figures 5(c) and (d)). The severe deformation of the Vit106a coupled with the elongation of the W powders in the shear plane resulted in a highly anisotropic open celled foam with pores elongated in a plane 24 to 27 deg from the horizontal plane of extrusion.

B. *Compressive Properties*

Although the three types of foams have the same range of porosity ($p = 57$ to 64 pct), their compressive mechanical properties vary greatly, reflecting the various extent of bonding between the Vit106a powders discussed previously. The VitCu foams are the weakest and least ductile, as a result of the poor bonding between the powders. The VitNi foams show strength and ductility improvements, reflecting the improved bonding between elongated powders. Finally, the VitW foams exhibit by far the highest strength and ductility, reflecting the better bonding of the Vit106a powders.

Figure 7 shows the compressive stress-strain curves reported previously for bulk Vit106a and the three

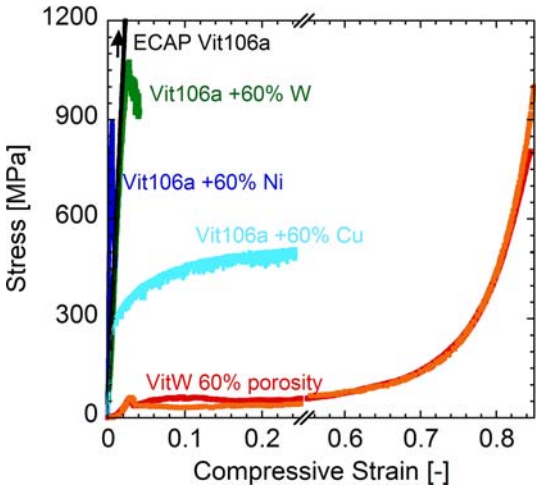

Fig. 7—Uniaxial compressive stress-strain curves of the Vit106a composites with 60 vol pct Cu, Ni, or W after ECAE consolidation, and the VitW foams created by dissolving the W phase of the Vit/W composite.

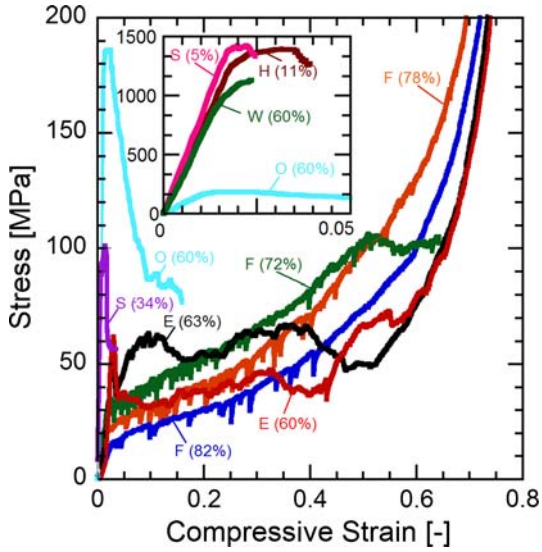

Fig. 8—Uniaxial compressive stress-strain curves for published Zr-based foams produced using He expansion (H, $p = 11$ pct),[37] W wire replication (W, $p = 60$ pct),[13] La_2O_3 replication (O, $p = 60.4$ pct),[12] spark plasma sintering (S, $p = 4.7$, 33.5 pct),[18] ECAE (E, $p = 59.5$ pct, 63 pct), and BaF_2 replication (F, $p = 72$ to 82 pct).[6] All foams, except H, have open porosity. All foams have equiaxed porosity, except for foams E and W, which have aligned, elongated pores.

Vit106a-Cu, -Ni, and -W composites produced by ECAE[25] and the present VitW foams produced by dissolution of the crystalline W phase from the Vit/W composite. The plasticity observed in the three composites is largely based on the ductility of the crystalline phase during room-temperature compression testing. For example, Cu has high ductility at room temperature, and thus dominates the plastic behavior of the Vit/Cu composite. Conversely, polycrystalline W has limited ductility at room temperature, and thus, the compressive plasticity observed in the Vit/W composite is likely the result of shear band propagation in the Vit106a phase and pinning of these shear bands by the crystalline W. While the strain to failure of the Vit/W composite ($\varepsilon_f = 2.2$ pct) is only marginally higher than that of the monolithic consolidated Vit106a ($\varepsilon_f = 1.7$ pct), no plasticity was observed in the monolithic sample before failure. Marked increases in compressive strains, along with concomitant strength decreases, are associated with the removal of the W phase, as illustrated in Figure 7. This opens the possibility of varying strength and ductility of the foams by only partially removing the metallic second phase, as previously achieved by a different processing method in syntactic Mg-based amorphous foams containing a steel second phase.[17]

Pore orientation has a marked affect on the strength and ductility of porous BMGs, as reported by Wada *et al.* for a Pd-based metallic glass foam with closed, aligned, elliptical pores having an aspect ratio of 3 and porosities $p = 3$ and 11 pct.[35] Compression samples for $p = 11$ pct with pores whose long axis is normal to the applied stress showed a higher plastic strain ($\varepsilon_f = 24$ pct) but a lower yield strength ($\sigma_y = 1070$ MPa) than foams with pores oriented parallel to the applied stress ($\varepsilon_f = 2$ pct and $\sigma_y = 1460$ MPa). The effects of pore orientation were explained by the stress concentration factor, which is lower for pores with their main axis parallel to the loading direction compared to those with a perpendicular axis. This high stress concentration in the former orientation results in a higher density of shear bands (emanating from the sharp extremities of the pores), which increases the macroscopic foam plasticity. A similar pore orientation study for ductile stainless steel foams ($p = 39$ pct) showed that, as the pore's long axis direction rotates away from that of the applied load, the yield stress decreases (by nearly a factor of 2 at a 90 deg rotation).[36]

Figure 8 compares compressive stress-strain curves for the present VitW foams, with those of previously published Zr-based BMG foams with equiaxed, open porosities ($p = 4.7$ to 78 pct) made by a variety of methods: He expansion,[37,38] spark plasma sintering of powders,[18] and salt replication.[6,12] Also shown in Figure 8 is a cast, amorphous Zr-based honeycomb produced by dissolution of aligned W wires within a Vit106a matrix,[13] with the resulting cylindrical pores ($p = 60$ pct) parallel to the axis of loading. Compressive yield strengths for the preceding Zr-based BMGs are compiled in Figure 9. The present VitW foams are also added to this figure, but cannot be directly compared to any of the other foams since their pore shape and orientation are different. However, it is apparent that the present VitW foams ($p = 59.5$ and 63 pct) with their relatively low strength and high compressive ductility are similar to the BaF_2 replicated foams ($p = 72$ to 82 pct).[6] Both types of foams show promising energy absorption capabilities: 32 to 38 MJ/m^3 for the present VitW foams and 16 to 44 MJ/m^3 for the BaF_2 replicated foams. These mechanical properties, together with the good corrosion and wear resistance and the low stiffness of the present VitW foams, make them also interesting as bone implant material.[39,40]

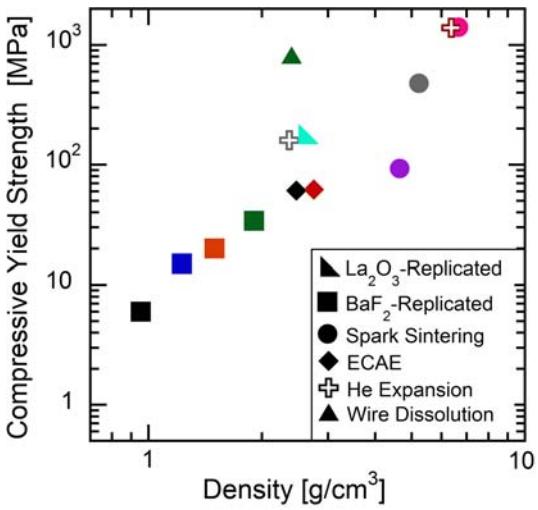

Fig. 9—Compressive yield strength as a function of density for porous Zr-based amorphous foams reported in Fig. 8.

Whereas the present VitW foams and the honeycomb structure produced by W wire dissolution both show aligned, highly elongated pores with similar porosity ($p = 59.5$ to 63 pct and 60 pct, respectively), they display yield strength differing by one order of magnitude (61 *vs* 820 MPa) and compressive ductility by two orders of magnitude (60 *vs* 0.6 pct). A first possible reason is the smaller pore width and length of the VitW foam (25- to 150-μm width and 80- to 350-μm length), as compared to those of the honeycomb structure (250-μm-diameter pore spanning the entire sample), since reducing feature size is known to increase ductility of BMG wire and foils.[41] The different pore orientation between the VitW foam and the honeycomb is another probable cause for the very different mechanical properties: the continuous unidirectional cylindrical pores aligned along the axis of loading induce buckling of the continuous thin walls spanning the full height of the foam, leading to catastrophic failure at low plastic strains and high stresses. In contrast, the aligned, elongated walls of the present VitW foam, because of their ~26 deg misalignment with respect to the loading direction, can bend at lower stress at multiple locations along their length, as also observed in the BaF_2 replicated foams with equiaxed pores.[6]

V. CONCLUSIONS

Equal channel angular extrusion was used to consolidate a blend of Zr-based BMG (Vit106a) and crystalline metal (Cu, Ni, or W) powders into dense composites. Chemical dissolution of the crystalline phase results in amorphous Vit106a foams with ~60 pct elongated pores, aligned at a 22 to 28 deg angle with respect to the compressive direction used during testing. Foams produced from composites with weak Cu exhibit a network of weakly bonded, somewhat elongated, Vit106a powders and a low peak compressive stress of 0.5 to 1 MPa. The codeformation of the Ni phase and the Vit106a produced foams with a network of elongated powders with improved mechanical bonding between Vit106a powders and higher yield stresses (6 to 14 MPa). Finally, foams produced from Vit/W composites show a fully densified Vit106a matrix with elongated pores, resulting in the highest compressive yield strength (62 MPa) and high energy absorbing capabilities (~36 MJ/m^3). As compared to traditional liquid processing, extrusion, or rolling methods, ECAE processing of composites/foams has the advantage of lower contamination risks and scalability while also providing higher flexibility for controlling second-phase/pore shape and orientation.

ACKNOWLEDGMENTS

One of the authors (MEC) was supported by a National Science Foundation Graduate Research Fellowship. The authors acknowledge the experimental help of Larry Jones, Materials Preparation Center, Ames Laboratory (United States Department of Energy), and Robert Barber of Texas A&M University.

REFERENCES

1. C.A. Schuh, T.C. Hufnagel, and U. Ramamurty: *Acta Mater.*, 2007, vol. 55, pp. 4067–4109.
2. A.L. Greer: *Mater. Today*, 2009, vol. 12, pp. 14–22.
3. E.S. Park and D.H. Kim: *Metall. Mater. Int.*, 2005, vol. 11, pp. 19–28.
4. D.C. Hofmann, J. Suh, A. Wiest, G. Duan, M. Lind, M.D. Demetriou, and W.L. Johnson: *Nature*, 2008, vol. 451, pp. 1085–89.
5. A.H. Brothers and D.C. Dunand: *Adv. Mater.*, 2005, vol. 17, pp. 484–46.
6. A.H. Brothers and D.C. Dunand: *Acta Mater.*, 2005, vol. 53, pp. 4427–40.
7. A. Brothers, D. Prine, and D.C. Dunand: *Intermetallics*, 2006, vol. 14, pp. 857–65.
8. A.H. Brothers and D.C. Dunand: *Scripta Mater.*, 2006, vol. 54, pp. 513–20.
9. A.H. Brothers and D.C. Dunand: *MRS Bull.*, 2007, vol. 32, pp. 639–43.
10. J. Schroers, C. Veazey, and W.L. Johnson: *Appl. Phys. Lett.*, 2003, vol. 82, pp. 370–72.
11. T. Wada and A. Inoue: *Mater. Trans., JIM*, 2004, vol. 45, pp. 2761–65.
12. T. Wada, F. Qin, X. Wang, A. Inoue, and M. Yoshimura: *Mater. Trans., JIM*, 2007, vol. 48, pp. 2381–84.
13. X.H. Chen, Y. Zhang, X.C. Zhang, X.D. Hui, B.C. Wei, and G.L. Chen: *Electrochem. Solid-State Lett.*, 2007, vol. 10, pp. E21–E23.
14. M.D. Demetriou, G. Duan, C. Veazey, K. De Blauwe, and W.L. Johnson: *Scripta Mater.*, 2007, vol. 57, pp. 9–12.
15. J. Jayaraj, B. Park, D. Kim, W. Kim, and E. Fleury: *Scripta Mater.*, 2006, vol. 55, pp. 1063–66.
16. A. Gebert, A.A. Kundig, L. Schultz, and K. Hono: *Scripta Mater.*, 2004, vol. 51, pp. 961–65.
17. A.H. Brothers, D.C. Dunand, Q. Zheng, and J. Xu: *J. Appl. Phys.*, 2007, vol. 102, art. no. 023508.
18. G. Xie, W. Zhang, D.V. Louzguine-Luzgin, H. Kimura, and A. Inoue: *Scripta Mater.*, 2006, vol. 55, pp. 687–90.
19. M.H. Lee and D.J. Sordelet: *Appl. Phys. Lett.*, 2006, vol. 89, art. no. 021921.
20. K. Qiu, B. Yu, and Y. Ren: *J. Univ. Sci. Technol. Beijing*, 2007, vol. 14, pp. 59–63.
21. M. Lee and D. Sordelet: *Scripta Mater.*, 2006, vol. 55, pp. 947–50.

22. M.D. Demetriou, J.P. Schramm, C. Veazey, W.L. Johnson, J.C. Hanan, and N.B. Phelps: *Appl. Phys. Lett*., 2007, vol. 91, art. no. 161903.
23. V.M. Segal: *Mater. Sci. Eng., A*, 1999, vol. 271, pp. 322–33.
24. I. Karaman, J. Robertson, J. Im, S. Mathaudhu, K. Hartwig, and Z. Luo: *Metall. Mater. Trans. A*, 2004, vol. 35A, pp. 247–56.
25. S.N. Mathaudhu, K.T. Hartwig, and I. Karaman: *J. Non-Cryst. Solids*, 2007, vol. 353, pp. 185–93.
26. J. Robertson, J.-T. Im, I. Karaman, K.T. Hartwig, and I.E. Anderson: *J. Non-Cryst. Solids*, 2003, vol. 317, pp. 144–51.
27. O. Senkov, S. Senkova, J. Scott, and D. Miracle: *Mater. Sci. Eng., A*, 2005, vol. 393, pp. 12–21.
28. S. Mathaudhu, J. Im, R. Barber, I. Anderson, I. Karaman, and K. Hartwig: *Supercooled Liquid Glass Transition and Bulk Metallic Glass*, Materials Research Society Symposium Proceeding, Warrendale, PA, 2003, vol. 754, pp. 191–98.
29. S. Schneider: *J. Phys.: Condens. Matter*, 2001, vol. 13, pp. 7723–36.
30. V.M. Segal: *Mater. Sci. Eng., A*, 1995, vol. 197, pp. 157–64.
31. S.J. Oh and S.B. Kang: *Mater. Sci. Eng., A*, 2003, vol. 343, pp. 107–15.
32. H.J. Frost and M.F. Ashby: *Deformation-Mechanism Maps: The Plasticity and Creep of Metals and Ceramics*, Pergamon Press, Oxford, NY, 1982, pp. 20–24 and 30–34.
33. Y. Kawamura, T. Shibata, A. Inoue, and T. Masumoto: *Scripta Mater*., 1997, vol. 37, pp. 431–36.
34. G.E. Dieter: *Mechanical Metallurgy*, McGraw-Hill, New York, NY, 1986, p. 297.
35. T. Wada, M. Kinaka, and A. Inoue: *J. Mater. Res*., 2006, vol. 21, pp. 1041–47.
36. T. Ide, M. Tane, T. Ikeda, S. Hyun, and H. Nakajima: *J. Mater. Res*., 2006, vol. 21, pp. 185–93.
37. T. Wada, X. Wang, H. Kimura, and A. Inoue: *Scripta Mater*., 2008, vol. 59, pp. 1071–74.
38. T. Wada, X. Wang, H. Kimura, and A. Inoue: *Mater. Lett*., 2009, vol. 63, pp. 858–60.
39. S.N. Parikh: *Orthopedics*, 2002, vol. 25, pp. 1301–09.
40. A.L. Greer, K.L. Rutherford, and M. Hutchings: *Int. Mater. Rev*., 2002, vol. 47, pp. 87–112.
41. R.D. Conner, W.L. Johnson, N.E. Paton, and W.D. Nix: *J. Appl. Phys*, 2003, vol. 94, pp. 904–11.